Supporting Information

Constructing MnO_2-$CuMn_2O_4$ interfaces to enhance the activation of surface lattice oxygen for efficient toluene combustion

Qiuyan Zhang, Yu Wu, Hongwei Jian, Aijie Wang, Haojie Yang, Chong Han*

School of Metallurgy, Northeastern University, Shenyang, 110819, China

Preparation of Comparative Catalysts

To systematically optimize the hydrothermal synthesis process of the catalyst, this study investigated the effects of key synthesis parameters. Firstly, a series of MnO_2/CMO samples was synthesized at different hydrothermal temperatures (120, 140, and 180 °C), while keeping all other steps consistent with the preparation method of MnO_2/CMO. Secondly, to determine the optimal amount of $KMnO_4$, the samples were prepared using $KMnO_4$ solutions with concentrations of 0.03 and 0.18 mol L^{-1}. The other preparation steps were identical to those for MnO_2/CMO.

To exclude the influence of water on CMO under hydrothermal conditions, the W-CMO catalyst was prepared. 0.6 g CMO was added to 50 mL deionized water and stirred at room temperature for 1 h. The suspension was transferred to a 100 mL Teflon-lined autoclave and heated to 160 °C for 3 h. The subsequent synthesis steps were identical to those of MnO_2/CMO.

To verify the interfacial effect of the interaction between MnO_2 and $CuMn_2O_4$, the Mix-M+C was synthesized by physically mixing the as-prepared MnO_2 and $CuMn_2O_4$ at the actual ratio of MnO_2 to $CuMn_2O_4$ in MnO_2/CMO (the ratio calculated by the ICP analysis).

Characterization methods

X-ray diffraction (XRD) was conducted using a D8 Advance powder diffractometer (Bruker,

* Corresponding author.

E-mail address: hanch@smm.neu.edu.cn (C. Han).

Germany). Raman spectroscopy was performed using an in Via confocal Raman microscope (Renishaw, UK) with an excitation wavelength of 532 nm. N_2 adsorption-desorption isotherm tests were performed by using a Nova 1200e analyzer (Quantachrome, USA) at 77 K. The Barrett-Joyner-Halenda (BJH) method was employed to determine pore size distributions. Inductively coupled plasma optical emission spectroscopy (ICP-OES) was performed on an Optima 8300DV instrument. Field emission scanning electron microscopy (FESEM) and energy dispersive spectrometer (EDS) were performed on an Ultra Plus (Zeiss, Germany) at an accelerating voltage of 20 kV. High-resolution transmission electron microscopy (HRTEM) images were recorded on a Tecnai G2 F20 (FEI, USA) at an accelerating voltage of 200 kV. X-ray photoelectron spectroscopy (XPS) was performed on an ESCALAB 250Xi electron spectrometer (Thermo Fisher Scientific, USA) with a monochromatic Al Kα source (hν = 1486.6 eV). The binding energies of all elements were referenced to the C 1s line at 284.8 eV from carbon impurities.

Temperature-programmed reduction and temperature-programmed desorption experiments were carried out on a chemical adsorption analyzer (ChemiMaster 8320, China). For hydrogen temperature-programmed reduction (H_2-TPR) experiments, 50 mg of sample was placed in a U-shaped quartz tube and pretreated at 200 °C for 1 h under Ar flows (30 mL min^{-1}). Then, the reduction of the samples was initiated from 50 to 900 °C (10 °C min^{-1}) in 5% H_2/Ar flow. Meanwhile, the H_2 consumption was recorded by a TCD while the temperature gradually increased to 900 °C. For the oxygen temperature-programmed desorption (O_2-TPD) measurement, 50 mg of the sample was pretreated in He flows (30 mL min^{-1}) at 200 °C for 1 h. The O_2 adsorption was conducted at 50 °C, with the exposure of 5% O_2/He (30 mL min^{-1}) for 60 min. After that, physically adsorbed O_2 was removed by He for 30 min. Finally, the O_2 desorption process was carried out in a He stream with temperatures linearly increasing from 50 to 900 °C (10 °C min^{-1}). The effluent gases were determined by an on-line mass spectrometer (PM-QMS, China). The signals at mass-to-charge (m/z) ratios of 32 (O_2) were detected. For the Toluene-TPD experiment, 50 mg of the sample was pretreated in He flows (30 mL min^{-1}) at 200 °C for 1 h. After the temperature cooled to 50 °C, the samples were placed in 1500 ppm of toluene for 1 h. The physically adsorbed toluene was removed by He for 30 min. Finally, the toluene desorption process was carried out in a He stream with temperatures

linearly increasing from 50 to 600 °C (10 °C min^{-1}). The toluene and CO_2 signals (m/z = 92, m/z = 44) were recorded using the MS detector. The toluene temperature-programmed surface reaction (Toluene-TPSR) involved the adsorption of toluene being saturated on the catalyst, followed by purging off the weakly adsorbed toluene with a He stream, and then heating in a 5% O_2/He flow from 50 to 600 °C (10 °C min^{-1}).

In situ diffuse reflectance infrared Fourier transform spectroscopy (DRIFTS, IS50, Thermo Fisher Scientific Inc., USA) was used to analyze toluene adsorption and oxidation mechanisms on catalysts. Before the experiment, the sample was treated in an N_2 flow (50 mL min^{-1}) at 250 °C for 1 h to remove surface impurities from the catalysts. In the temperature-dependent experiment, the background spectra were collected in the N_2 atmosphere at room temperature. The gas flow was then switched to a reaction gas containing 500 ppm toluene (20% O_2 + N_2) at the same flow rate. The spectra of the products formed on the catalyst surface were continuously recorded as the catalyst was heated to 160 °C, 180 °C, 200 °C, 220 °C and 240 °C. To evaluate the lattice oxygen activity and gaseous oxygen activation levels of the catalysts, the catalysts were exposed to an atmosphere containing 500 ppm toluene under both oxygen-free and air conditions, and the accumulation of intermediates was monitored by *in situ* DRIFTS. The water resistance stability experiment was conducted under an air atmosphere containing 1.5 vol% water and 500 ppm toluene.

DFT calculations

All spin-polarized density functional theory calculations were conducted by the Vienna Ab initio simulation package (VASP). The exchange-correlation potential was described by using the generalized gradient approximation of Perdew-Burke-Ernzerhof (GGA-PBE). Dispersion interactions were described using the Grimme DFT-D3 method. The ion cores and valence electrons were depicted by the projector augmented-wave (PAW) method, and the plane-wave cutoff energy was set to 450 eV. The Monkhorst-Pack k-points grid was specified as 1 × 1 × 1 during the calculations. The given structural models were optimized until the Hellmann-Feynman forces were smaller than −0.02 eV/Å and the energy change was less than 10^{-5} eV. The (220) crystal plane of $CuMn_2O_4$ was chosen as the most stable plane for calculation. The model consisted of 16 Cu atoms and 32 Mn atoms. For MnO_2, the (001) crystal plane was

selected as the most stable plane, with a model consisting of 4 Mn atoms and 8 O atoms. Only one side of the exposed surface was permitted for the adsorption.

The oxygen vacancy formation energy (E_{VO}) was calculated as:

$$E_{VO}=E_d-E_p+E_{O_2/2}$$

where E_d and E_p are the energy of the defective and perfect slab surface, respectively. $E_{O_2/2}$ is the energy of gaseous oxygen molecule.

The adsorption energy (E_{ads}) of A (toluene and O_2) on the catalysts were calculated as:

$$E_{ads}=E_{A/catalyst}-E_{catalyst}-E_A$$

where $E_{A/catalyst}$ and $E_{catalyst}$ are the energy of the catalyst with A adsorption and without A adsorption, respectively. E_A is the energy of gaseous toluene or oxygen molecules.

The Density of States (DOS) projected onto the d-states that interact with the adsorbate state was characterized by the moments of the d-PDOS, with the first moment representing the d-band center:

$$\text{d-band center} = \int_{\infty}^{\infty} n_d(\varepsilon)\varepsilon d\varepsilon / \int_{\infty}^{\infty} n_d(\varepsilon)d\varepsilon$$

where $n_d(\varepsilon)$ and ε refer to the electron density and electron energy with respect to the Fermi level, respectively. The calculation method for the p-band center follows a similar formula.

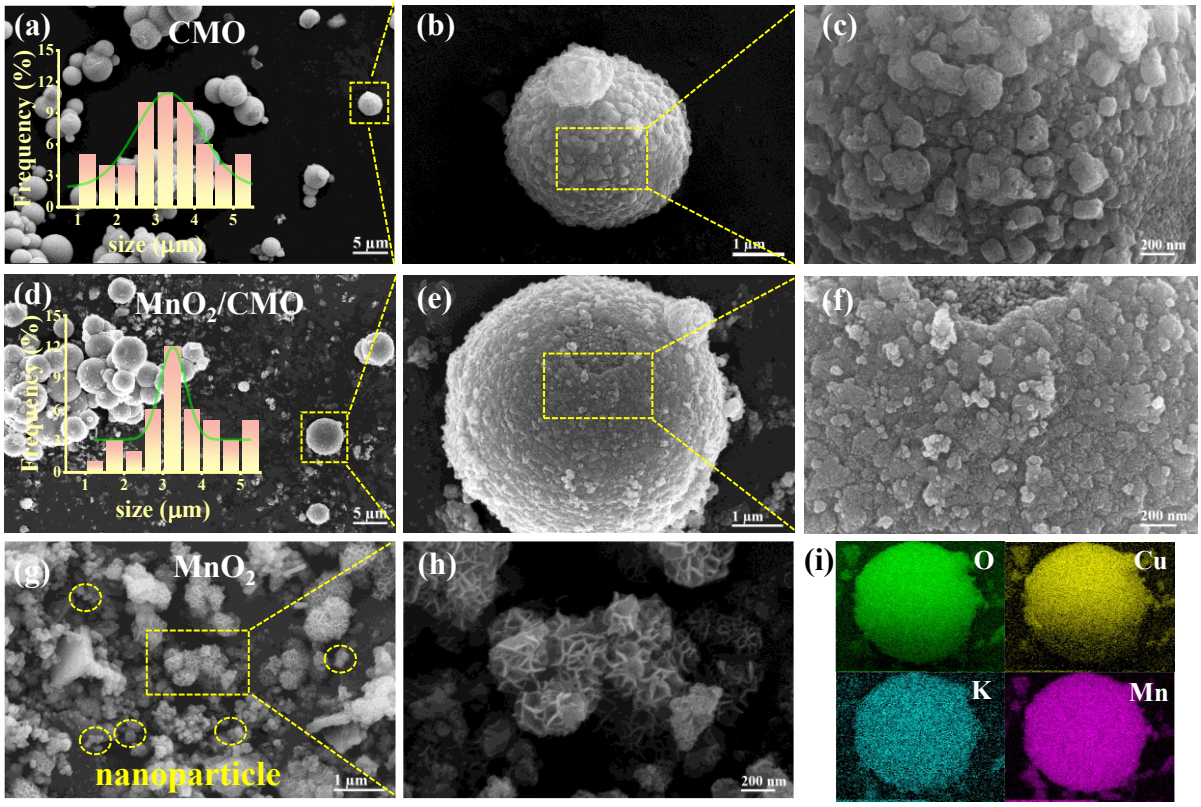

Fig. S1 SEM images of CMO (a, b, c), MnO_2/CMO (d, e, f) and MnO_2 (g, h); (i) elemental mapping images of MnO_2/CMO.

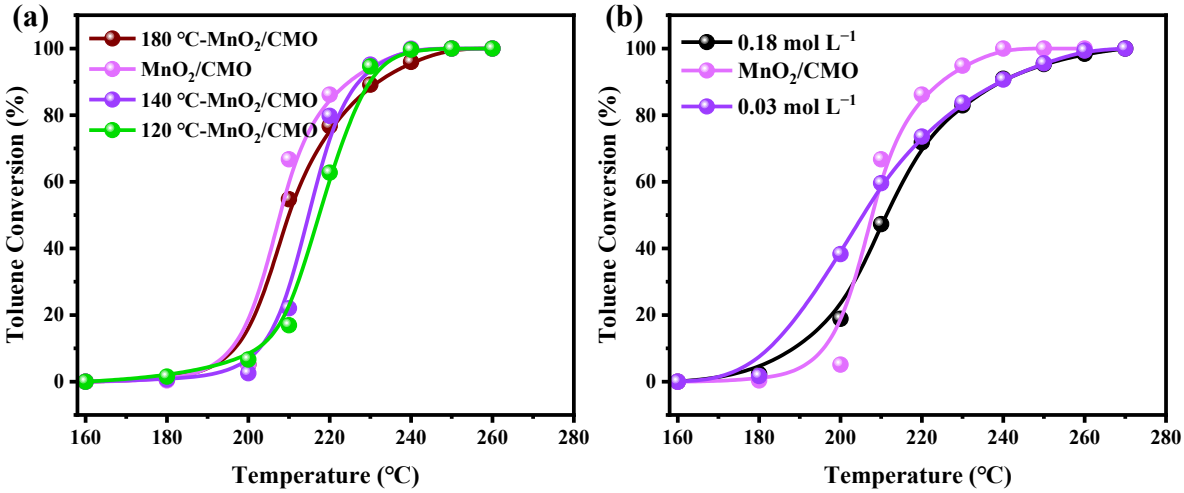

Fig. S2 Catalytic combustion performance of toluene on the catalysts prepared at different (a) hydrothermal temperatures and (b) $KMnO_4$ concentrations.

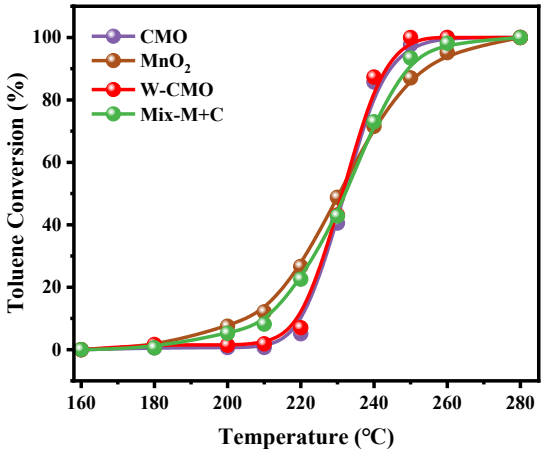

Fig. S3 Conversion of toluene by various catalysts.

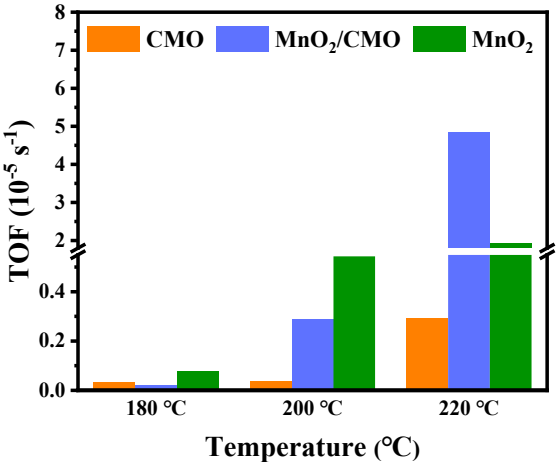

Fig. S4 Turnover frequency (TOF) of catalysts.

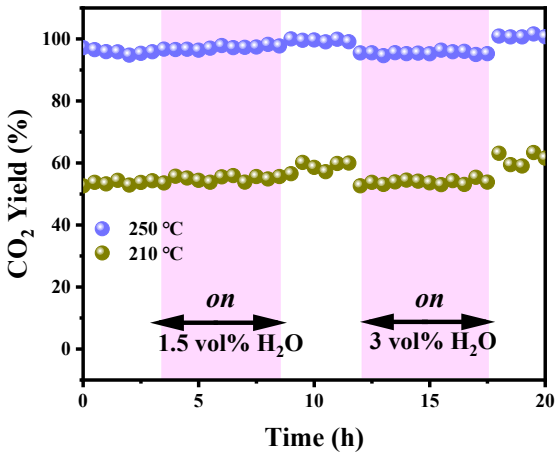

Fig. S5 Effect of water vapor on CO_2 yield of MnO_2/CMO.

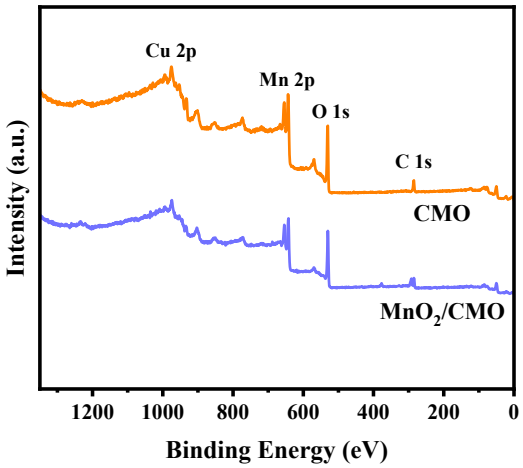

Fig. S6 XPS survey spectra of CMO and MnO_2/CMO.

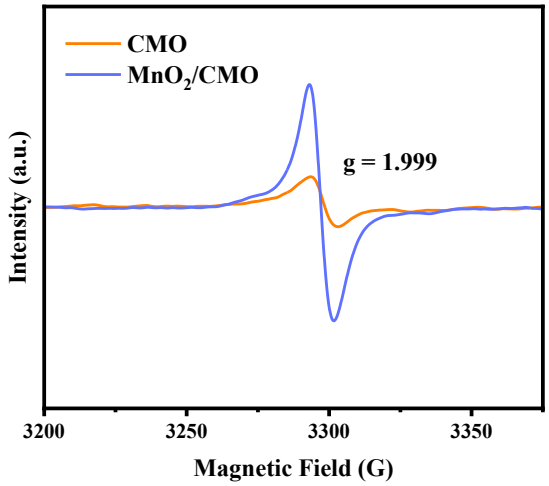

Fig. S7 EPR spectra of CMO and MnO_2/CMO.

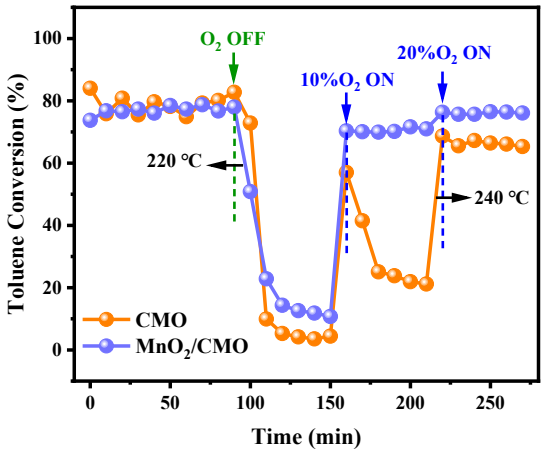

Fig. S8 Toluene conversion of CMO and MnO_2/CMO in O_2-free reaction as a function of time.

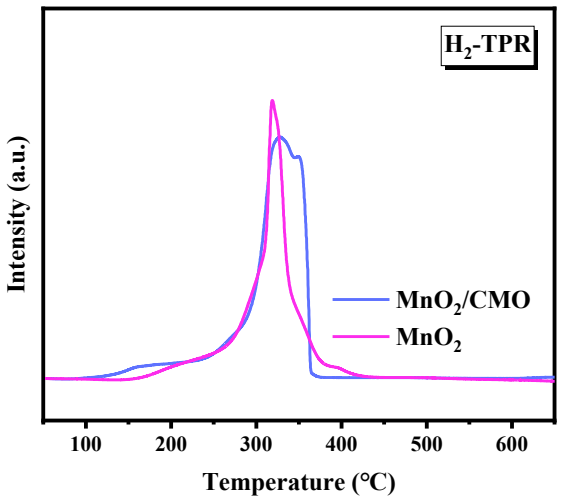

Fig. S9 H_2-TPR profiles of CMO and MnO_2/CMO.

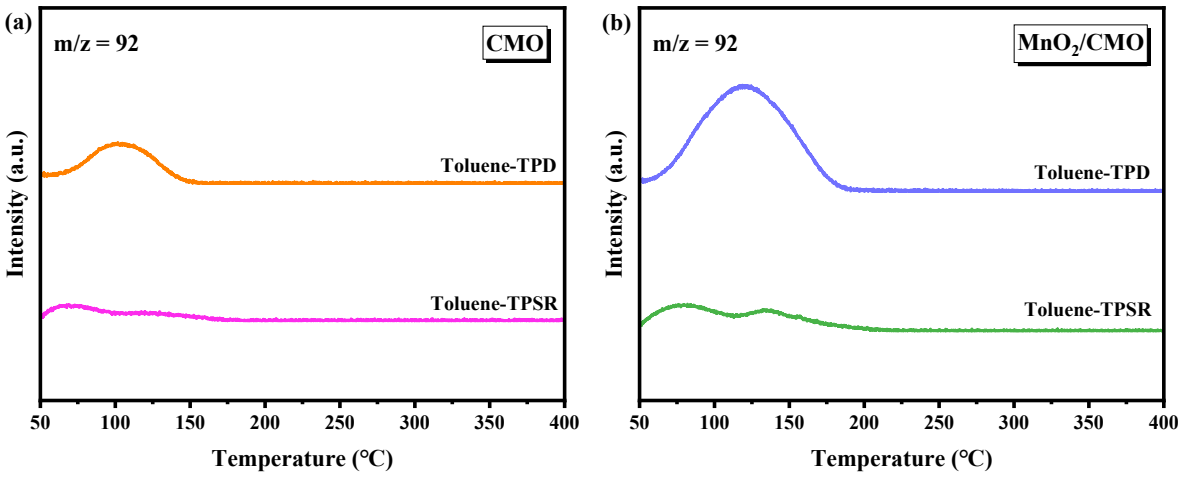

Fig. S10 Toluene MS signals of CMO (a) and MnO_2/CMO (b) during Toluene-TPD and Toluene-TPSR experiments.

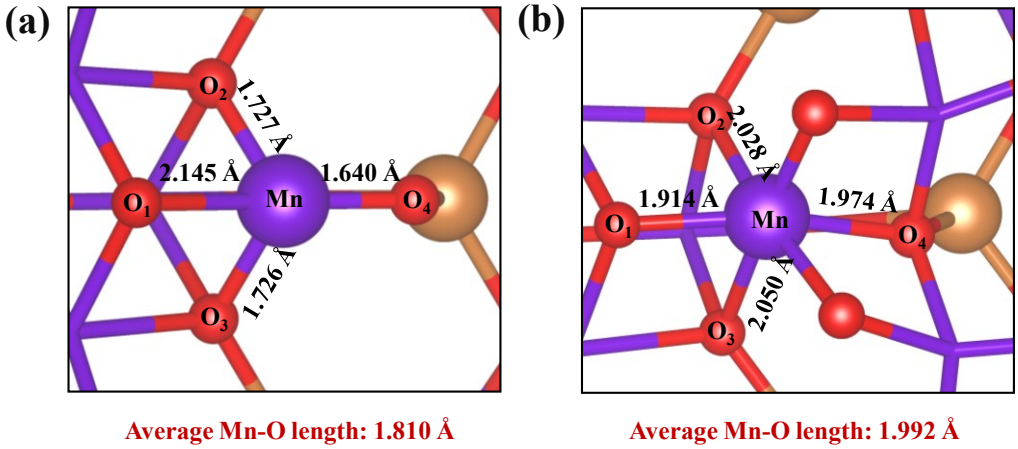

Fig. S11 Mn-O bond length of CMO (a) and MnO_2/CMO (b).

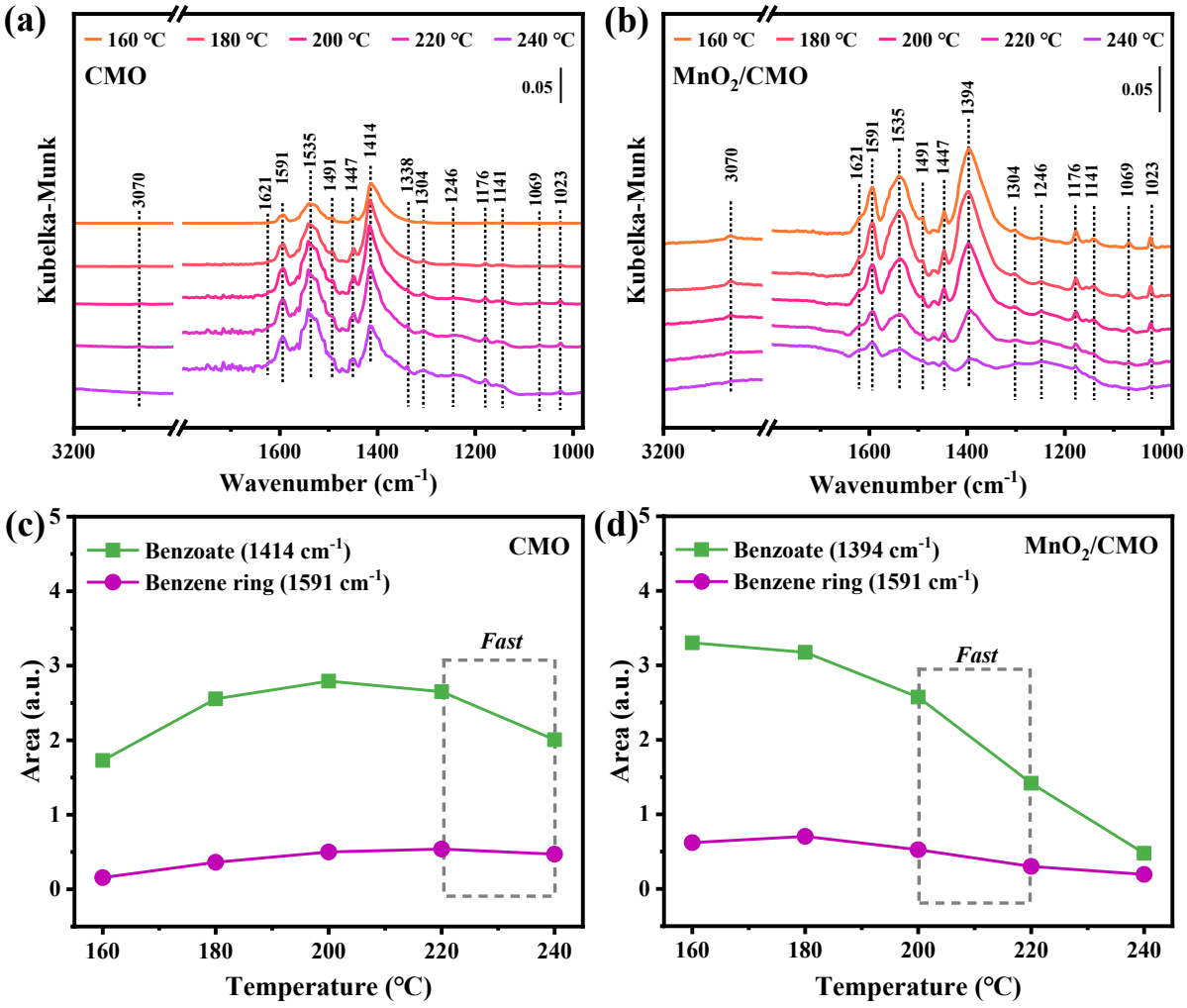

Fig. S12 (a, b) *In-situ* DRIFTS spectra and (c, d) plots of consumption of benzene ring and benzoate over CMO and MnO_2/CMO during toluene oxidation from 160 to 240 °C.

Table S1 EDS, ICP analysis of the catalysts.

Sample	EDS (wt%)				ICP (wt%)			
	Cu	Mn	K	K/MnO_2 atomic ratio	Cu	Mn	K	K/MnO_2 atomic ratio
CMO	22.3	40.24	/	/	28.25	39.77	/	/
MnO_2/CMO[a]	20.4	46.1	1.62	0.25	24.1	44.6	1.69	0.22
MnO_2	/	47.28	7.92	0.24	/	51.5	9.92	0.21

[a]It was assumed that the MnO_2/CMO only consisted of $CuMn_2O_4$ spinel and MnO_2 phases.

Table S2 The catalytic oxidation activities of VOCs by the reported catalysts.

Catalysts	VOCs	Concentration (ppm)	GHSV (mL g^{-1} h^{-1})	$T_{90\%}$ (°C)	Ref.
MnO_2/CMO	toluene	1000	60,000	223	This work
CFO-N-I	toluene	1000	30,000	280	1
Co_1/MnO_2	toluene	1000	60,000	260	2
CuO-MnO_x	toluene	1000	60,000	225	3
Co_3O_4/Fe−S	toluene	100	15,000	256	4
CMO-AC45	toluene	1000	60,000	~245	5
Mn_2O_3-T-0.5	toluene	1000	60,000	252	6
4% Ag/MnO_2	toluene	1000	20,000	~215	7
Ag/δ-MnO_2	toluene	1000	60,000	224	8
Au/3DOM Mn_2O_3	toluene	1000	40,000	244	9

Table S3 Summary of XPS analysis results.

Sample	Cu^{+}/Cu	Mn^{4+}/Mn^{3+}	AOS[a]	$O_V/(O_L + O_V)$
CMO	0.39	0.33	3.281	0.376
MnO_2/CMO	0.18	0.65	3.314	0.393

[a]The AOS of Mn was accurately calculated by the equation: AOS = 8.956 − 1.126ΔE, where ΔE denoted the binding energy difference of two peaks for Mn 3s.

Table S4 The valence band center of Cu 3d, Mn 3d and O 2p on catalysts.

Sample	Cu 3d	Mn 3d	O 2p
CMO	−1.94 eV	−1.14 eV	−3.10 eV
MnO_2/CMO	−1.73 eV	−1.05 eV	−2.89 eV

References

1 D. Zhu, Y. Huang, R. Li, S. Peng, P. Wang and J. Cao, *Environ. Sci. Technol.*, 2023, **57**, 17598–17609.

2 M. Jiang, D. Yan, X. Lv, Y. Gao and H. Jia, *Appl. Catal. B.*, 2022, **319**, 121962.

3 S. Xiong, N. Huang, Y. Peng, J. Chen and J. Li, *J. Hazard. Mater.*, 2021, **415**, 125637.

4 R. Li, Y. Huang, Y. Zhu, M. Guo, W. Peng, Y. Zhi, L. Wang, J. Cao and S. Lee, *Environ. Sci. Technol.*, 2024, **58**, 14906–14917.

5 Y. Yang, W. Si, Y. Peng, J. Chen, Y. Wang, D. Chen, Z. Tian, J. Wang and J. Li, *Appl. Catal. B.*, 2024, **340**, 123142.

6 W. Yang, Y. Peng, Y. Wang, Y. Wang, H. Liu, Z. Su, W. Yang, J. Chen, W. Si and J. Li, *Appl. Catal. B.*, 2020, **278**, 119279.

7 Y. Qin, Y. Wang, J. Li and Z. Qu, *Surf. Interf.*, 2020, **21**, 100657.

8 W. Yang, X. Zhao, Y. Wang, X. Wang, H. Liu, W. Yang, H. Zhou, Y. A. Wu, C. Sun, Y. Peng and J. Li, *Catal. Sci. Technol.*, 2022, **12**, 5932–5941.

9 S. Xie, H. Dai, J. Deng, H. Yang, W. Han, H. Arandiyan and G. Guo, *J. Hazard. Mater.,* 2014, **279**, 392–401.